JOURNAL OF CATALYSIS 81, 224–238 (1983)

Decomposition of Formic Acid on Copper, Nickel, and Copper–Nickel Alloys

III. Catalytic Decomposition on Nickel and Copper–Nickel Alloys

E. IGLESIA[1] AND M. BOUDART[2]

Department of Chemical Engineering, Stanford University, Stanford, California 94305

Received April 28, 1982; revised December 7, 1982

Turnover rates for the catalytic dehydrogenation and dehydration of formic acid (HCOOH) on Ni/SiO_2 and Ni and CuNi powders between 390 and 490K are reported. The decomposition rate constants calculated from these data are compared with values reported previously for the temperature-programmed decomposition (TPD) of HCOOH preadsorbed on Ni and CuNi. On these, catalytic dehydrogenation and dehydration seem to proceed through the same intermediate, believed to be a formate ion. The selectivity S, defined as the ratio of dehydrogenation to dehydration turnover rates, is independent of temperature, and between 4 and 6 on Ni and alloys with a surface Cu fraction less than 0.8. The observed selectivity is not affected by secondary reactions among the products. The intermediate appears to be bound to two adjacent Ni atoms. In contrast, TPD of HCOOH preadsorbed at low coverage on CuNi single crystals seems to involve a formic anhydride species that requires four adjacent Ni atoms, and decomposes with S equal to unity and a rate constant 5×10^3 times greater than that corresponding to the catalytic decomposition. Differences between catalytic and TPD data apparently arise from the effect of surface coverage on the relative surface density of formate and formic anhydride. Formate requires small nickel ensembles and predominates on fully covered surfaces typical of the catalytic reaction. This study demonstrates the differences in rate constant and S when reactive intermediates change with surface coverage because they require different ensembles for adsorption; in other words, they are structure sensitive.

INTRODUCTION

Recent studies of the temperature-programmed decomposition (TPD) of formic acid (HCOOH) preadsorbed on Ni(110) (*1–3*) and Ni(100) (*4*) single crystals concluded that the products of the reaction arise from the decomposition of formic anhydride (HCOOOCH) to equal amounts of CO_2, CO, and H_2. On adlayer-covered Ni(110), a formate species (HCOO), decomposing exclusively via dehydrogenation, was also detected (*5–8*). The ratio of formate to anhydride increased with increasing C (*5*), O (*6*), and Cu (*7, 8*) surface density because the formation of formic anhydride required a larger number of adjacent Ni atoms. Therefore, the selectivity S, defined as the ratio of CO_2 to CO in the decomposition products, increased with increasing density of C, O, or Cu at the Ni surface.

Only formate has been detected by adsorption measurements and infrared spectroscopy during the catalytic decomposition of HCOOH on Ni (*9–12*), and following its adsorption at room temperature on Ni (*13–19*). The vibrational spectra and composition of these species are identical to those of bulk Ni formate. The selectivity is between 2.5 and infinity (*20–51*). The catalytic decomposition on CuNi alloys leads exclusively to dehydrogenation products (*23, 25, 27, 43*). In this study, the turnover

[1] Present address: Corporate Research Science Laboratories, Exxon Research and Engineering, Linden, N. J., 07036.

[2] To whom inquiries should be addressed.

0021-9517/83 $3.00
Copyright © 1983 by Academic Press, Inc.
All rights of reproduction in any form reserved.

rate N and selectivity S of the zero-order decomposition of HCOOH on Ni/SiO_2, Ni/Al_2O_3, and Ni and CuNi powders, in the absence of side reactions and other artifacts, are reported. These data are compared with those reported in TPD studies. A similar comparison for the decomposition of HCOOH on Cu was previously reported (*52*).

EXPERIMENTAL

The preparation and characterization of the catalysts used in this study are reported elsewhere (*53*). Supported Ni was prepared by impregnation ($Ni(wt\%)/SiO_2$). CuNi powders were prepared by coprecipitation of the metal carbonates, calcination in air to the mixed oxides, and reduction in dihydrogen (*54*). The Ni dispersion and the surface composition of the alloys were calculated from the surface density of strongly adsorbed hydrogen (*53*).

The apparatus and the experimental procedure used in this study have been previously reported (*52*). Before the rate measurements, prereduced and passivated catalysts were rereduced for 2 h at 723K in flowing Pd-diffused H_2 (Liquid Carbonic) at a site-contact frequency of 4–10 s^{-1}. The site- (or bulk) contact frequency ν^s_M (or ν^b_M) is defined as the number of M molecules entering the reactor per unit time per surface (or bulk) metal atom. Dehydrogenation and dehydration turnover rates were calculated from the concentration of CO_2 and CO, respectively, in the carrier stream, measured by gas chromatography. The turnover rate is reported per Ni surface atom on Ni, and per total surface atom on the alloys. In the latter, the total number of surface metal atoms was obtained from the total surface area of the samples, measured by BET dinitrogen physisorption with 0.162 nm^2 per N_2 molecule, assuming a surface density of 1.5×10^{15} cm^{-2}. Typical HCOOH fractional conversions and site-contact frequencies are 0.0001–0.5 and 0.1–6.0 s^{-1}, respectively. Formic acid partial pressures were between 1 and 6 kPa.

RESULTS

Decomposition Kinetics

On Ni and CuNi alloys, the site-time yield was independent of CO_2 and H_2 concentration, but it decreased with increasing CO and decreasing HCOOH pressure in the carrier gas. The site-time yield is defined as the number of product molecules appearing at the reactor outlet per unit time per surface metal atom. It decreases with increasing HCOOH conversion. The turnover rates calculated from these data are described by

$$N_i = N_{0,i}[1 + (K_i(CO)/(HCOOH))]^{-1} \quad (1)$$

for both the dehydrogenation and dehydration reactions. Zero-order turnover rates, N_0, were calculated by extrapolation of the data to zero conversion or CO pressure.

On Ni the observed selectivity, S_0, defined as the ratio of CO_2 to CO in the decomposition products, is independent of conversion and CO and HCOOH pressure. Therefore, it equals the zero-order selectivity,

$$S = (N_{0,CO_2}/N_{0,CO}), \quad (2)$$

because the inhibition factor, K_i, is identical for both reactions. Ni-rich alloys behaved similarly. However, on Cu-rich alloys, S_0 depends on conversion and CO and HCOOH pressure because the decomposition on Ni ensembles, leading to CO_2 and CO, depends on these, while that on Cu ensembles, leading only to CO_2, does not. The zero-order selectivity on these alloys was obtained by extrapolation to zero conversion or CO pressure.

Decomposition on Oxidized Samples

The rate of decomposition of HCOOH at 503K and 1.5 s^{-1} HCOOH site-contact frequency on Ni powders preexposed to O_2, ($\nu^b_{O_2} = 43$ h^{-1}, 673K, 3 h) was initially negligible. The site-time yield and S increased with time. After 13 h, the site-time yield was only 10% of the value before O_2 exposure. The selectivity increased from 4 to 5.5

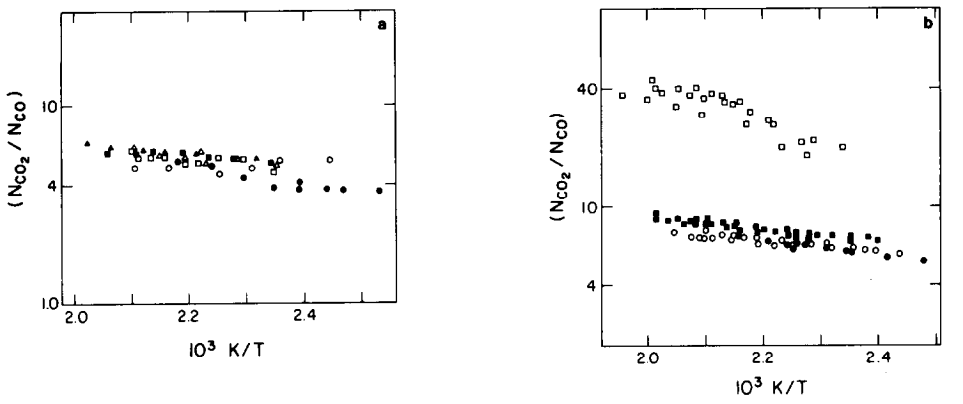

FIG. 1. Decomposition selectivity. (a) Nickel-rich alloys (Cu atomic surface fraction follows each symbol). ○, 0.0; ●, 0.0; □, 0.55; ■, 0.61; ▲, 0.73; △, 0.77. (b) Copper-rich alloys. ●, 0.78; ○, 0.81; ■, 0.91; □, 0.97.

in this time, compared with a value of 6 before O_2 exposure. Reduction of the sample in H_2 ($\nu^s_{H_2}$ = 4–10 s^{-1}, 723K, 0.5 h) restored the initial rate and selectivity (±10%). The reduction of CuNi samples preexposed to O_2 by the decomposition reaction products was much more rapid than on pure Ni. The initial site-time yield was restored within 0.25–0.5 h during HCOOH decomposition at 490–510K on 0.05 and 0.95 Cu bulk atomic fraction alloys.

Zero-Order Decomposition Data

Copper–nickel powders. The activation energy and preexponential factor for the catalytic dehydrogenation and dehydration of HCOOH on CuNi powders are shown in Table 1. Dehydration and dehydrogenation activation energies are very similar, and do not vary with surface composition. Consequently, S is almost independent of temperature and surface composition (Fig. 1).

TABLE 1

Activation Energy (E) and Preexponential Factor (A) for the Zero-Order Catalytic Decomposition of Formic Acid on Copper–Nickel Powders

Cu atomic bulk fraction	Cu atomic surface fraction[a]	Dehydrogenation		Dehydration	
		E (kJ mol^{-1})	$\log(A)$ (s^{-1})[b]	E (kJ mol^{-1})	$\log(A)$ (s^{-1})[b]
0.00	0.00	100.2	11.55	93.0	10.05
0.005	0.55	100.3	11.06	95.7	9.92
0.05	0.61	101.2	11.10	99.1	10.06
0.10	0.73	105.3	11.44	102.0	10.30
0.25	0.77	99.1	10.60	92.0	9.03
0.50	0.78	99.6	10.71	95.3	9.41
0.70	0.81	104.5	11.10	99.1	9.65
0.90	0.91	96.2	10.06	92.6	8.67
0.95	0.97	98.6	10.08	84.0	7.00
1.00	1.00	96.6	9.82	—	—

[a] From dihydrogen uptake measurements (*53*).
[b] Per total number of metal surface atoms.

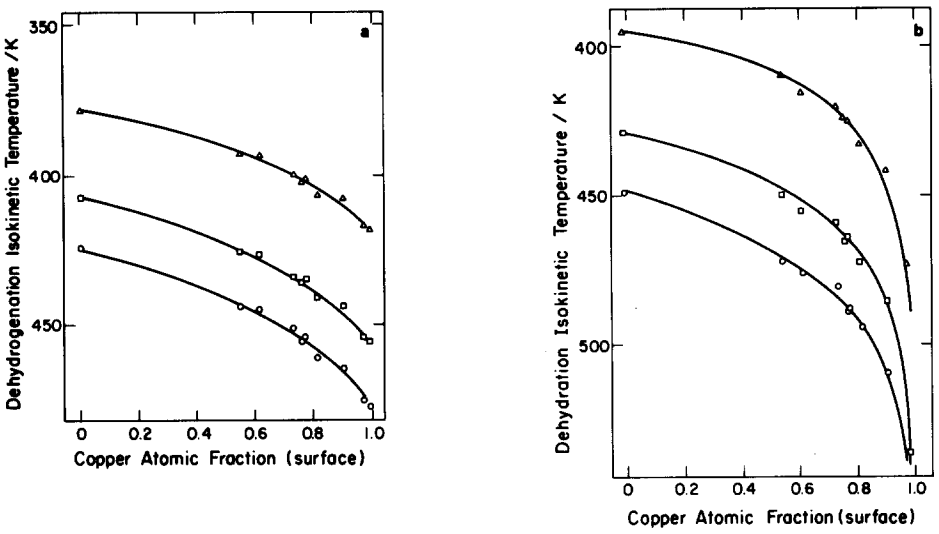

FIG. 2. Isokinetic temperature vs surface composition of CuNi powders. (a) Dehydrogenation, (b) dehydration (N (s^{-1}) follows each symbol). △, 0.005; □, 0.05; ○, 0.16.

The effect of surface composition on the dehydrogenation and dehydration isokinetic temperature is shown in Fig. 2. The isokinetic temperature T_0 is defined as that required for the reaction to occur with a given turnover rate. For both reactions, the isokinetic temperature increases with increasing copper content.

The dehydrogenation turnover rate at 455K is 10 times greater on Ni than on Cu (Fig. 3). Both dehydrogenation and dehydration rates decrease faster than linearly with increasing Cu surface fraction. Therefore, the rate per Ni surface atom decreases slightly with alloying. The selectivity is between 4.5 and 6. It is independent of surface composition except for Cu-rich alloys (Fig. 6). Up to 0.8 Cu surface fraction, the reaction products arise from the decomposition of intermediates adsorbed on the more active ensembles (Ni), and the selectivity is identical to that on pure Ni. Only at higher Cu surface fraction does the lower, but exclusively dehydrogenating, activity of Cu ensembles affect S.

Nickel. The activation energy and preexponential factor for the catalytic dehydrogenation and dehydration of HCOOH on Ni powders and supported Ni are shown in Table 2. The turnover number for each reac-

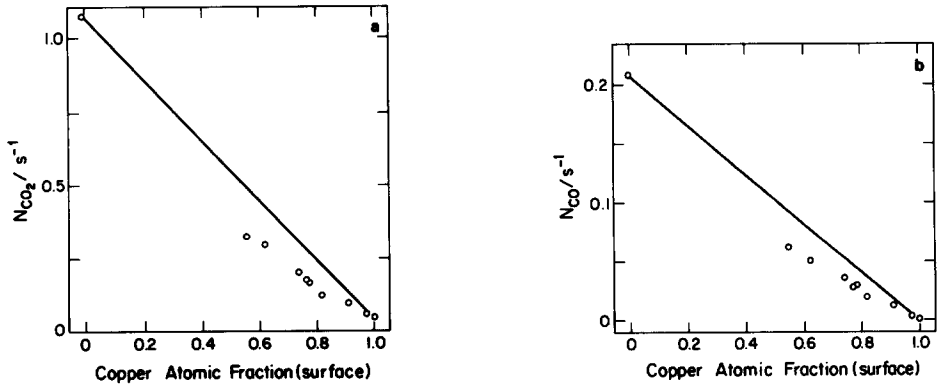

FIG. 3. Zero-order turnover rate vs surface composition of CuNi powders (455K). (a) dehydrogenation, (b) dehydration.

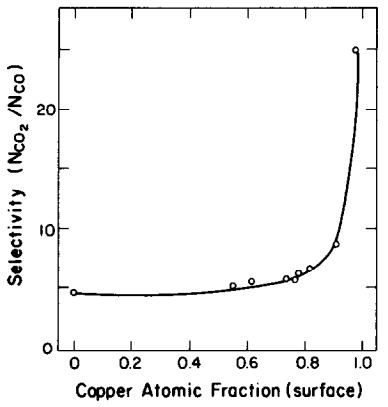

FIG. 4. Formic acid decomposition selectivity vs surface composition of CuNi powders (445K).

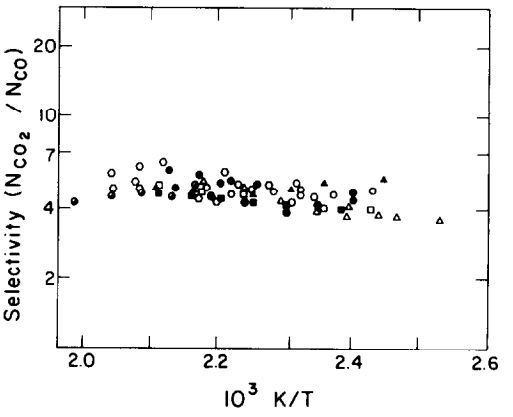

FIG. 5. Formic acid decomposition selectivity on nickel. ●, Ni(2.2)/SiO_2; ○, Ni(8.5)/SiO_2; ■, Ni(11.3)/SiO_2; □, Ni(22.0)/SiO_2; ▲, Ni; △, Ni; ⬢, Ni(A); ○, Ni(5.0)/Al_2O_3; ◕, bulk nickel formate (Ref. (*60*)).

tion is slightly higher on powders than on supported catalysts, but S is identical and almost independent of temperature on all samples (Fig. 7). The activation energy is similar on all samples. The turnover number increased slightly with increasing metal loading and decreasing metal dispersion on silica-supported Ni.

Below 400K, the decomposition site-time yield on Ni decreased steadily with time (50–100% in 3 h), but S remained unchanged. Turnover rates reported in this study were measured above 400K.

DISCUSSION

The turnover rate expression (Eq. (1)) is consistent with a reaction sequence involving the decomposition of a common intermediate, believed to be a formate ion, to dehydrogenation and dehydration products on a surface covered by CO and formate. The kinetically significant steps in such a reaction sequence are

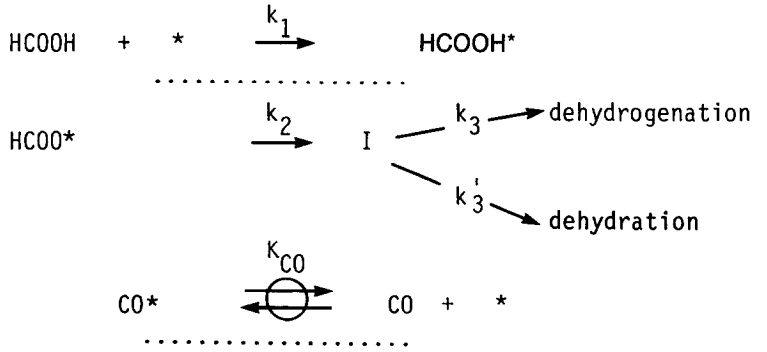

(3)

where * represents an active surface site. The steady-state approximation, with CO* and HCOO* as the most abundant surface intermediates, leads to a turnover rate expression identical to Eq. (1), with

$$K = (K_{CO}k_2/k_1), \tag{4}$$

$$N_{0,CO_2} = k_2P, \tag{5a}$$

$$N_{0,CO} = k_2(1 - P), \tag{5b}$$

where P is the probability that the intermediate I will dehydrogenate:

$$P = k_3(k_3 + k_3')^{-1}. \tag{6}$$

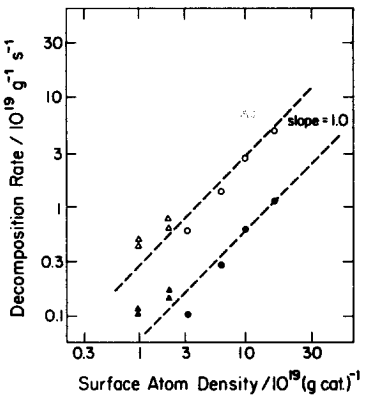

FIG. 6. Koros–Nowak test. Catalytic decomposition of formic acid on Ni (435K). Open symbols, dehydrogenation; solid symbols, dehydration. Ni powder, △, ▲; Ni/SiO_2, ○, ●.

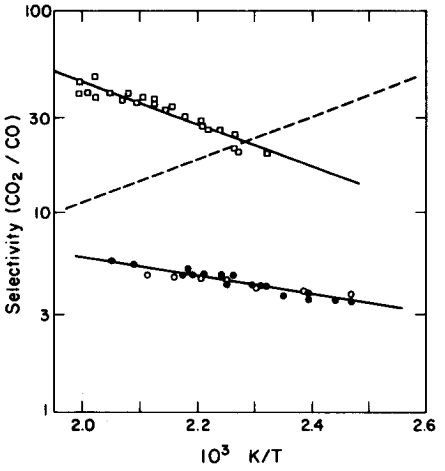

FIG. 7. The role of the water-gas shift reaction* in the catalytic decomposition of formic acid on Ni and CuNi. ●, Ni powder; ○, $Ni(11.3)/SiO_2$; □, CuNi powder (0.98 Cu surface atomic fraction); ——, water-gas shift equilibrium. * $CO + H_2O \rightleftharpoons CO_2 + H_2$.

The selectivity is then given by

$$S = (k_3/k_3'). \qquad (7)$$

It is independent of CO and HCOOH pressure, as observed experimentally.

The reactive intermediate I may resemble adsorbed CO_2, formed from formate ions by hydrogen cleavage. Thereafter it may desorb or dissociate to CO and adsorbed oxygen, leading to dehydrogenation and dehydration products, respectively. Water is subsequently formed by the reaction of adsorbed H and O atoms. The weak temperature dependence of S is surprising in view of the drastically different rearrangements involved in the two decomposition paths.

The expression for N (Eq. (1)) will be treated as an empirical equation, useful in

TABLE 2

Activation Energy (E) and Preexponential Factor (A) for the Zero-Order Catalytic Decomposition of Formic Acid on Nickel Catalysis

Catalyst	wt% nickel	Dispersion[a]	Dehydrogenation		Dehydration	
			E (kJ mol^{-1})	log(A) (s^{-1})[b]	E (kJ mol^{-1})	log(A) (s^{-1})[b]
Ni/SiO_2	2.2	0.13	104.5	11.7	103.5	10.8
Ni/SiO_2	8.5	0.104	105.5	12.0	104.5	11.2
Ni/SiO_2	11.3	0.083	107.0	12.3	100.0	10.8
Ni/SiO_2	22.0	0.078	106.0	12.1	105.0	11.4
Ni[c]	100	0.0017	97.0	11.2	85.5	9.2
Ni[c]	100	0.0015	103.0	11.9	100.5	10.8
Ni[d]	100	—	100.0	11.6	93.0	10.0
Ni(A)	100	0.00066	111.0	13.0	111.0	12.4
Ni/Al_2O_3[e]	5.0	—	103.0	—	105.0	—

[a] From dihydrogen uptake measurements (*53*).
[b] Per nickel surface atom (Ni : H = 1 : 1).
[c] Decomposition reaction on two batches of similarly prepared nickel.
[d] Average kinetic parameters from the two decomposition runs.
[e] No dispersion data available, only small fraction of total dihydrogen uptake was irreversibly adsorbed.

the minor extrapolations required to calculate turnover rates from site-time yield-conversion data.

Previous studies of the effect of the reaction products on the catalytic HCOOH decomposition rate on Ni yielded contradictory results. Some authors (*37, 55, 56*) reported that it was not affected by preadsorption of CO_2 or H_2O, but CO preadsorption decreased, and H_2 preadsorption increased the decomposition rate. Other authors (*26*) observed a decrease in rate with conversion in batch reactors. Increasing CO_2 or H_2 pressure decreased the rate slightly, but CO and H_2O had no effect. However, on Raney nickel CO_2 or H_2 pressure had no effect on the rate (*34*).

The inhibiting effect of CO reported here is consistent with detection of adsorbed CO by infrared spectroscopy on Ni surfaces during catalytic HCOOH decomposition at 300–400K (*16, 18, 57*). The CO band intensity increased with temperature and HCOOH conversion (*16, 57*). Carbon and oxygen were detected on Ni(110) surfaces following molecular beam studies of HCOOH decomposition (*58*). The presence of adsorbed CO is also predicted from the heat of adsorption of CO on Ni (*59*).

The reduction of bulk NiO by the products of HCOOH decomposition at 503K is shown by the increase in site-time yield with time. Similar effects were previously reported, albeit at higher decomposition temperature (*35, 40*). Oxygen preadsorbed on Ni(110) is partially removed by adsorption and subsequent HCOOH TPD (*6*). In this work (*6*), the effect of adsorbed oxygen is to increase the ratio of formate to anhydride, and thus S. In the present study, reduction of NiO during decomposition was accompanied by an increase in S.

Irreversible changes in N and S during the catalytic decomposition of HCOOH on Ni were previously reported (*26, 27*), but probably resulted from impurities in the reactant and secondary reactions among the primary products. In this study, N and S on Ni and CuNi above 400K did not change with time. Below 400K, on pure Ni, N decreased with time. It may be attributed to sintering by interparticle transport of volatile nickel carbonyl at low temperature, or to an increase in the steady-state density of adsorbed oxygen atoms, resulting from a decrease in the rate of their removal by hydrogen adatoms with decreasing temperature (*60*).

Turnover Rate, Selectivity, and Reactive Intermediates

The HCOOH dehydrogenation turnover rate decreases faster than linearly with increasing Cu surface fraction on CuNi powders. At 455K, N is 10 times greater on Ni than on Cu. On alloys, it is proportional to the Ni surface fraction to a power between 1 and 2. Turnover rate data are described by

$$N = x^2_{Ni}N_{Ni} + 2x_{Ni}x_{Cu}(N_{Ni}N_{Cu})^{1/2} + x_{Cu}{}^2N_{Cu}, \quad (8)$$

where N_{Ni} and N_{Cu} are the turnover rates on pure Ni and Cu, respectively, and x_{Ni} and x_{Cu} their fraction at the alloy surface. This expression suggests that the reactive intermediate is bound to two adjacent metal surface atoms, and that N, proportional to the decomposition rate constant of these intermediates, depends on the identity of the two metal atoms in the binding ensemble. In contrast, formic anhydride requires ensembles consisting of four adjacent Ni atoms (*7, 8*).

The values of N measured on pure Ni correspond to the rate constant of the surface-catalyzed reaction, devoid of any effects of rate-limiting transport processes, such as heat or mass transfer, secondary reactions, or catalyst bed bypassing or channeling. This was demonstrated by the successful application of the Koros–Nowak criterion (Fig. 6) (*61, 62*). The test involves the measurement of identical turnover rates on Ni/SiO_2 catalysts with different metal loading. The slope of unity in the logarithmic plot of decomposition

rate per gram of catalyst as a function of the density of surface Ni atoms in the bed (Fig. 6) demonstrates the absence of artifacts. The similar activation energy measured on all Ni and CuNi catalysts also shows that the rate constant of the catalytic decomposition of HCOOH on Ni is that of the surface-catalyzed steps. Similar results were previously reported for the catalytic HCOOH decomposition on Cu (*52*).

The effect of surface composition on the dehydration and dehydrogenation turnover rates on CuNi powders is similar (Fig. 3), except HCOOH dehydration is not observed on pure Cu. Again, the reactive intermediate is bound to two adjacent surface metal atoms, and the dehydration rate constant depends on the identity of the ensemble atoms.

The similarity in binding ensembles required for the intermediates leading to dehydrogenation and dehydration products leads to identical S on pure Ni and all CuNi powders with surface Cu fraction less than 0.8 (Fig. 4). On these, the products arise exclusively from the decomposition of intermediates bound to Ni–Ni and perhaps Cu–Ni ensembles, which are the most reactive, and on which S is identical to its value on pure Ni surfaces. This suggests that the catalytic decomposition of HCOOH is not sensitive to ligand effects of neighboring Cu atoms on Ni ensembles. Only at higher Cu surface fraction are the products of the dehydrogenation of HCOOH on Cu ensembles observed, and S increases with increasing Cu surface fraction.

The selectivity on Ni and CuNi alloys with less than 0.8 copper surface fraction is between 4.5 and 5.5 throughout the experimental temperature range. It is much greater than that predicted for the decomposition of formic anhydride ($S = 1.0$). The constant value of S suggests that dehydration and dehydrogenation of HCOOH on Ni occur through the same intermediate, which is not formic anhydride.

The constant value of S with alloying is not caused by chemisorption-induced segregation of Ni to the alloy surface during HCOOH decomposition, which may result in a pure Ni surface on most CuNi powders. Dehydrogenation and dehydration turnover rates decrease by a factor of 4 in this composition range, showing that a large fraction of the Ni surface atoms are replaced by Cu in the alloys. Chemisorption-induced formation of a pure Ni surface was not observed during H_2 or O_2 chemisorption on Ni(100) and Ni(110) at 573K (*63*). The binding energy of formate at the Ni surface is intermediate between that of these two species, and the catalytic decomposition reaction was studied below 483K. Although thermodynamically favored, the chemisorption-induced formation of a pure Ni surface was also not observed during H_2 chemisorption on CuNi powders at room temperature (*53*). Furthermore, changes in surface composition were never reported during TPD of HCOOH preadsorbed on CuNi alloys (*7, 8, 64*). Apparently, chemisorption-induced segregation is limited by low diffusion rates at these temperatures.

The value of S is very similar on Ni powders and SiO_2- and Al_2O_3-supported Ni (Fig. 5). It depends only weakly on temperature, suggesting again a similar intermediate and decomposition mechanism for both reactions. The intermediate is believed to be a formate ion. Indeed, S for the catalytic decomposition of HCOOH on Ni is identical to that measured during the isothermal decomposition of bulk Ni formate (Fig. 5) (*60*). The latter S was also independent of conversion, concentration of reaction products, and temperature (*60*).

Studies using TPD suggest that formate ions adsorbed on Ni at low surface density only dehydrogenate (*5–8*). If this also applies to the catalytic reaction, the observed products must arise from mixtures of formate and formic anhydride surface species. Therefore, S would change markedly with surface composition, because formic anhydride, the exclusive source of CO, requires larger ensembles; thus its surface density decreases more markedly with alloying

than that of formate. The catalytic S, however, is independent of surface composition. Therefore, formate ions may dehydrate as well as dehydrogenate during catalytic HCOOH decomposition on Ni.

The catalytic S (4.5–5.5) is higher than that predicted for the decomposition of formic anhydride (1.0) on Ni, but identical to values observed during isothermal decomposition of bulk Ni formate (Fig. 5) (*60*). The differences may arise from secondary interconversions among the primary decomposition products. Indeed, different values of S reported for HCOOH decomposition on Ni are often attributed to side reactions, such as the water-gas shift (*65*) and the reverse reaction (*26, 27*), the formation of adsorbed oxygen (*4, 6, 18, 33*) and carbon (*5, 66*), and HCOOH decomposition on supports or reactor walls (*24*). Some authors have proposed that CO and H_2O are the only primary products of HCOOH decomposition on Ni (*30, 65*); dehydrogenation products were attributed to the water-gas shift. Other authors observed that S increases with time and conversion in a static reactor; they proposed that HCOOH only dehydrogenates on Ni, the dehydration products resulting from the reverse water-gas shift reaction (*26*). The amount of CO in the decomposition products was, however, greater than that predicted from the equilibrium of this reaction; therefore, CO is a primary decomposition product.

In this study, additional evidence for the primary nature of CO and CO_2 is presented. The selectivity is independent of metal loading in supported catalysts, and therefore of the density of active sites in the reactor bed; thus secondary reactions are ruled out (*60, 61*). In addition, S on Ni powders and on SiO_2- and Al_2O_3-supported Ni is much lower than that predicted from the water-gas shift equilibrium (Fig. 7). Therefore, CO is a primary product of HCOOH decomposition on Ni; it is not formed from the reverse water-gas shift reaction. In contrast with TPD studies, formate decomposition under catalytic conditions yields dehydration and dehydrogenation products. The reaction between CO_2 and H_2 on Ni yields CH_4 and H_2O exclusively (*67*). Methane was never observed during HCOOH decomposition on Ni or CuNi.

The absence of the water-gas shift reaction and the primary nature of CO_2 and H_2 products are also demonstrated in Fig. 7. On Cu-rich alloys, S is higher than that predicted from the water-gas shift equilibrium. Cu is a much better catalyst for this reaction than Ni (*68*), but even on Cu-rich alloys S is not affected by this reaction. Extrapolation of reported water-gas shift turnover rates on Ni and Cu (*68*) to HCOOH decomposition conditions shows they are less than 0.05 and 0.3% of the HCOOH decomposition turnover rate on Ni and Cu, respectively, even in the absence of coadsorbed HCOOH. Therefore, catalytic HCOOH decomposition on Ni does not occur through a formic anhydride intermediate decomposing with S equal to unity, followed by interconversion of products by water-gas shift.

Comparison with Previous Data

Catalytic. In contrast with similar values of N and S reported by various workers for the catalytic decomposition of HCOOH on Cu (*52*), the data reported on Ni catalysts differ markedly (Table 3). Many authors report only dehydrogenation, while others report values of S between 2.5 and 10. Only a few of these studies were accompanied by metal surface area measurements; areal rates were often reported on the basis of geometric area.

Dehydrogenation isokinetic temperatures reported here are lower than most values previously reported (Table 3). Activation energies are similar to the higher values reported previously. Some of the low values of activation energy and N previously reported may have been affected by rate-limiting transport processes. Values of dehydration turnover rate and activation energy on Ni were never reported.

TABLE 3

Catalytic Decomposition of Formic Acid on Ni. Summary of Literature Data

Catalyst	T (K)	A^a (s^{-1})	E (kJ mol^{-1})	T_i^b (K)	S^c	Ref.
Wire	530–630	—	125.5	—	—	*74*
Wire	453–533	—	104.5	—	∞	*48*
Powder	—	—	120	—	∞	*39*
Powder	673–743	3×10^7	101	630	∞	*40*
Raney	350–383	1.6×10^6	64	473	∞	*34*
Ni/SiO_2	343–423	1×10^{10}	96.5	463	18–33	*16*
Ni/SiO_2	343–423	—	95–102	—	—	*10*
Powder	573–673	1.5×10^8	86.5	500	∞	*41*
Powder	573	—	103	—	—	*29*
Ni/TiO_2	573	—	78–94	—	10	*29*
Ni/Cr_2O_3	573	—	83	—	—	*29*
Ni/Al_2O_3	468–523	—	85	—	—	*36*
Ni/TiO_2	468–523	—	96	—	—	*36*
Powder	468–523	—	111	—	—	*36*
Foil	463	—	96	—	—	*37*
Powder	413–443	2×10^{10}	100.5	466	∞	*33*
Film	398–462	3×10^7	66	415	3	*26*
—	523	—	—	—	2.5–3.5	*30*
Foil	456–483	—	114	—	16	*29*
Powder	483	—	—	—	13.5	*31*
Foil	603–693	—	83.5	—	∞	*35*
Film	400–460	—	69	—	—	*22*
Powder	400–460	—	57	—	—	*22*
Foil	393–473	—	48.5	—	—	*25*
Foil	473–673	—	106.5–108.5	—	∞	*38*
Foil	523–573	1.3×10^{12}	125.5	505	∞	*43*
Powder	353–473	4×10^{10}	101	464	∞	*44*
Film	473	—	101	—	∞	*23*
Powder	453	9×10^9	96	465	—	*46*
Foil	453	—	79.5–83.5	—	—	*46*
Film	373–573	1.6×10^7	70	455	2.5	*27*
Powder	323–373	—	103.5	—	∞	*28*
Ni/Al_2O_3	—	—	23.5	—	—	*47*
Film	523–653	—	111	—	—	*49*
Ni/Al_2O_3	523–653	—	85.5	—	—	*49*
Film	453	—	82.5–85	—	—	*50*
Sheet	373–493	—	83.5–94	—	—	*51*
Powder dehydrogenation	400–500	4×10^{11}–1×10^{13}	100–111	418–420	3.5–5.5	This study
Powder dehydration	400–500	1×10^{10}–2×10^{12}	93–111	438–447		This study
Ni/SiO_2 dehydrogenation	400–500	5×10^{11}–2×10^{12}	104.5–107	425–434	4–5.5	This study
Ni/SiO_2 dehydration	400–500	6×10^{10}–2.5×10^{11}	100–105	447–461		This study
Ni/Al_2O_3	400–500	—	103 (dehydrogenation) 105 (dehydration)		4–5	This study

[a] Per surface Ni atom, assuming a surface density of 1.5×10^{15} cm^{-2}.

[b] Temperature at which a turnover rate of 0.16 s^{-1} is measured.

[c] Ratio of CO_2 to CO in reaction products.

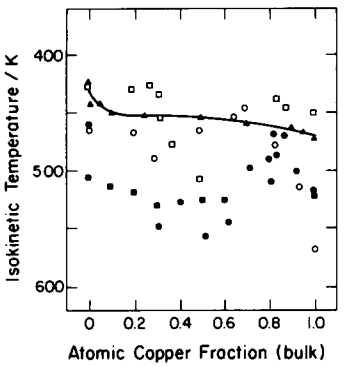

FIG. 8. Formic acid dehydrogenation isokinetic temperature on CuNi ($N = 0.16\ s^{-1}$). Comparison with previous data. ▲, This study, powders; ●, Rienacker and Bade (*25*), foils; ○, Quinn and Taylor (*44*), powders; ■, Dowden and Reynolds (*43*), foils; □, Alsdorf and Volter (*23*), films.

Isokinetic temperatures for HCOOH dehydrogenation on CuNi powders reported here are compared with previous data on CuNi foils, films, and powders (*23, 25, 27, 43*) in Fig. 8. Previous studies did not report surface compositions; therefore, the data are compared on the basis of bulk copper content. None of these authors reported HCOOH dehydration on CuNi alloys.

Temperature-programmed decomposition. Decomposition rate constants and S obtained from TPD of HCOOH preadsorbed on Ni, adlayer-covered Ni, and CuNi alloys are shown in Tables 4 and 5.

On Ni, the surface density of adsorbed formic anhydride never exceeds 2×10^{14} cm^{-2} (*1–4*). At low HCOOH exposures typical of preadsorption in TPD experiments, the "saturation" surface density depends on the value at which the adsorption sticking coefficient becomes smaller than about 0.01. In contrast, formate surface coverages exceeding one monolayer are found during HCOOH decomposition on Ni powder (*9*). The preexponential factor for formic anhydride decomposition on Ni is much greater than that for the decomposition of the most abundant surface intermediate in the catalytic HCOOH decomposition, suggesting a larger entropy of activation for the former. The activation energy for formic anhydride decomposition is similar to that measured for the catalytic reaction (Tables 3 and 4). However, it is very sensitive to surface coverage because of attractive interactions among anhydride

TABLE 4

Temperature-Programmed Decomposition of Formic Acid Preadsorbed on Ni. Summary of Literature Data

Metal	Desorbing species	A (s^{-1})	E (kJ mol^{-1})	S^a	Saturation coverage (10^{15} cm^{-2})	Ref.
Ni(110)	CO_2	—	99.5	0.3 (low θ)	0.18	*1*
	H_2	—	99.5	1.0 (saturation)	0.18	*1*
	CO	1.6×10^{15}	111	—	0.18	*1*
Ni(110)	CO_2, H_2	6×10^{15}	$106.5 + 11.3\theta$	1.0	—	*4*
Ni(100)	CO_2, H_2	6×10^{15}	$106.5 + 5.8\theta$	1.0	0.20	*4*
	CO	1×10^{15}	109	—	0.20	*4*
Ni(110) (2 × 1)C	CO_2, H_2	4×10^{12}	106.5	3–10	0.15	*5*
Ni(100) p(2 × 2)C	CO_2, H_2	8×10^{14}	118.5	∞	0.4	*66*
Ni(110)	CO_2, H_2	1.6×10^{12}	84.5	3	0.16	*6*
(2 × 1)O	CO	4×10^{12}	106	—	0.05	*6*
Ni(110)	HCOO* → CO_2	1×10^{11}	72	2.5	10^{-4}	*58*
MBRS	HCOO* → CO*	5×10^{10}	72	—	—	*58*
	CO* → CO	7×10^{12}	96.5	—	—	*58*

[a] Ratio of CO_2 to CO in decomposition products.

TABLE 5

Temperature-Programmed Decomposition of Formic Acid Preadsorbed on CuNi(110) (Refs. (*7*) and (*8*))

Cu surface fraction[a]	Dehydrogenation		S^c	T_i^d (K)
	E (kJ mol^{-1})	A^b (s^{-1})		
0	100.5	1×10^{15}	1.0	332
0.13	103.0	5×10^{15}	1.3	325
0.26	105.0	1×10^{15}	1.8	346
0.32	103.0	5×10^{14}	2.3	345
0.39	108.0	1×10^{15}	2.9	357
0.44	—	—	3.9	—
0.50	—	—	5.5	—
0.63	107.5	4×10^{14}	8.4	368
1.0	133.3	9×10^{13}	∞	484

[a] Measured from the intensity of low-energy (100-eV) Auger transitions of Cu and Ni.

[b] From heating rate variation, assuming decomposition rate is first order in adsorbed intermediate.

[c] Ratio of CO_2 to CO products after preadsorption of HCOOH at saturation coverage.

[d] Isokinetic temperature calculated assuming a surface density of intermediates of 10^{15} cm^{-2} (k = 0.16 s^{-1}).

species (*4*), which lead to surface islands and autocatalytic decomposition of formic anhydride (*1*, *4*). Formic anhydride decomposes with S equal to unity and a rate constant 5×10^3 greater than that measured for the decomposition of surface formate in catalytic experiments.

The ratio of formate to formic anhydride on Ni(110) increases with increasing Cu (*7*, *8*), carbon (*5*), and oxygen (*6*) surface concentration. The selectivity is very sensitive to alloying (Fig. 9a), because of the larger ensemble required for the binding of formic anhydride than of formate. In contrast, the catalytic S is independent of surface Cu content over a wide composition range, because the reactive intermediate does not change with alloying. In TPD studies, the effects of C and Cu on selectivity are explained by an ensemble effect (*69*) resulting from the decrease in the average size of nickel surface ensembles with alloying.

The decomposition rate constant measured in TPD experiments is also much more sensitive to alloying than the catalytic rate constant (Fig. 9b). The TPD rate constant is an average of those for the decomposition of formic anhydride and formate on Ni ensembles, and thus changes dramatically as the ratio of the surface density of these two species changes with alloying. In contrast, the catalytic rate constant corresponds to the decomposition of the most reactive surface species. Its surface density

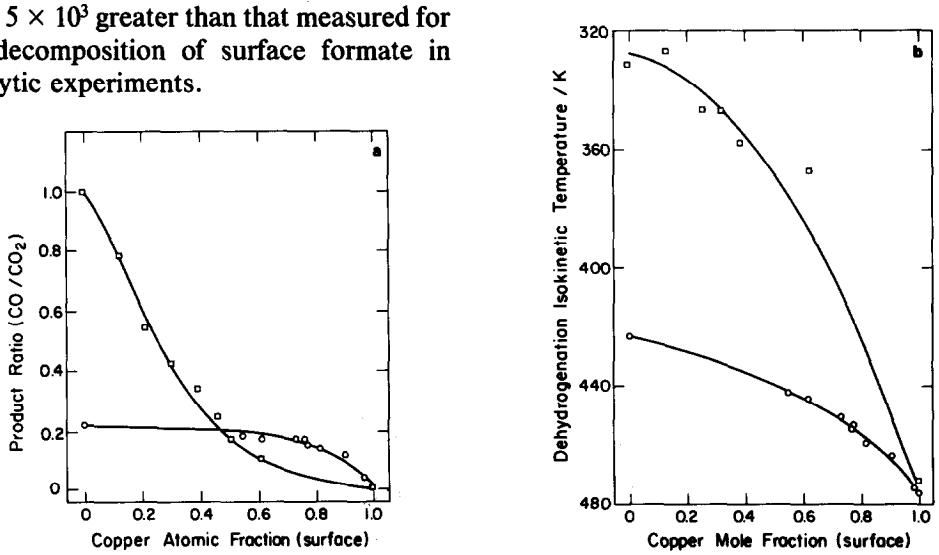

FIG. 9. The effect of surface composition on the selectivity and isokinetic temperature of formic acid decomposition on CuNi. Comparison of TPD and catalytic data. (a) Selectivity (445K), (b) isokinetic temperature (k = 0.16 s^{-1}). ○, This study, catalytic decomposition, CuNi powders; □, Ying and Madix (*7*, *8*), TPD, CuNi(110).

decreases with alloying, but its identity and decomposition selectivity are unchanged. The differences in isokinetic temperatures calculated from TPD and catalytic data decrease with increasing Cu content, because the identity of the surface intermediates giving rise to the decomposition products are similar for the two studies on Cu-rich but not on Ni-rich alloys.

Surface Science and Catalysis

The different rate constants and selectivity obtained from TPD of preadsorbed HCOOH and catalytic HCOOH decomposition on Ni and CuNi alloys arise from differences in intermediate and decomposition mechanisms, apparently caused by the large surface density of coadsorbed species typical of the zero-order catalytic decomposition.

The decomposition products arise from a formate rather than a formic anhydride intermediate during the catalytic reaction possibly because

(i) the large surface density of adsorbed species during the catalytic decomposition of HCOOH reduces the number of four-atom Ni ensembles required for the formation of formic anhydride; adsorbed species may be formate, carbon, oxygen or decomposition products;

(ii) the rate constant for the decomposition of formic anhydride decreases with increasing surface density, as a result of attractive interactions among these species, and of a decrease in the activation entropy gain allowed in the formation of the decomposition transition state on a fully covered surface.

Because the products of the catalytic decomposition of HCOOH are formed only from the most reactive intermediate, the latter effect may explain the absence of products of the decomposition of formic anhydride in the catalytic reaction, but not the absence of formic anhydride bands in infrared studies during catalytic HCOOH decomposition on Ni (*10–12*).

The ensemble effect reported for the decomposition of HCOOH preadsorbed on CuNi(110) (*7, 8*) and adlayer-covered Ni(110) (*5, 6*) should also be observed at high HCOOH surface coverage, since increasing density of adsorbed species decreases the average size of the available Ni ensembles. The ensemble effect is identical to that of alloying as long as the lifetime of adsorbed formate is long compared to that of unoccupied Ni ensembles, as in the zero-order catalytic decomposition of HCOOH on Ni.

The conclusions of this study are not affected by whether the adsorbed species are coadsorbed intermediates, or surface carbon or oxygen layers formed during the catalytic reaction. If present, these are inherent byproducts of the catalytic reaction, which prevent the attainment of the value of S reported during TPD of HCOOH preadsorbed on Ni.

The absence of dehydration products in TPD of formate ions on adlayer-covered Ni (*5, 6*) and CuNi alloys (*7, 8*) is not consistent with

(i) the detection of strong infrared bands corresponding to formate ions, but no anhydride bands, following the adsorption of HCOOH on Ni/SiO_2; formate decomposition resulted in significant amounts of dehydration products (*11, 12, 16*);

(ii) the observation of dehydration products (S = 3–4) during the decomposition of bulk Ni formate (*60, 70, 71*);

(iii) the formation of CO_2 and CO from formate species during molecular beam studies of the decomposition of HCOOH on Ni(110) (*58*).

Dehydration of formate ions on metal surfaces probably leads to the formation of adsorbed oxygen, which remains at the surface following TPD of preadsorbed HCOOH. Indeed, this was observed during the decomposition of HCOOH preadsorbed on Fe (*72*), W (*73*), and Ni (*4*). In the former two, dehydration products arose from the decomposition of a formate surface species. Under catalytic conditions,

partial or complete removal of the adsorbed oxygen may occur by reaction with coadsorbed hydrogen. The steady-state oxygen surface density and the decomposition selectivity then depend on the relative rates of oxygen adsorption and removal and thus on the binding energy of oxygen atoms at the metal surface. Dehydration is apparently possible only on metal surfaces with sufficiently high oxygen binding energy.

In summary, catalytic dehydrogenation and dehydration of HCOOH on Ni and CuNi alloys occur through the same intermediate, believed to be a formate ion. The decomposition rate constant and S are different from those predicted for a formic anhydride intermediate. In contrast with previous results for HCOOH decomposition on Cu (*52*), the rate constant and S calculated from TPD of HCOOH preadsorbed on Ni are different from those of the corresponding step in the catalytic decomposition sequence. The value of S observed during the decomposition of HCOOH preadsorbed at low surface coverage on Ni single crystals is not observed during the catalytic decomposition of HCOOH on Ni.

REFERENCES

1. McCarty, J., Falconer, J., and Madix, R. J., *J. Catal.* **30,** 235 (1973).
2. Falconer, J. L., and Madix, R. J., *Surf. Sci.* **46,** 473 (1974).
3. Falconer, J. L., and Madix, R. J., *J. Catal.* **51,** 47 (1978).
4. Benziger, J. B., and Madix, R. J., *Surf. Sci.* **79,** 47 (1978).
5. McCarty, J., and Madix, R. J., *J. Catal.* **38,** 402 (1975).
6. Johnson, S. W., and Madix, R. J., *Surf. Sci.* **66,** 189 (1977).
7. Ying, D. H. S., and Madix, R. J., *J. Inorg. Chem.* **17,** 1103 (1978).
8. Ying, D. H. S., Ph.D. dissertation, Stanford University, 1978.
9. Tamaru, K., *Trans. Faraday Soc.* **55,** 824 (1959).
10. Fahrenfort, J., and Hazebroek, H. F., *Z. Phys. Chem.* **20,** 105 (1959).
11. Fahrenfort, J., van Reijen, L. L., and Sachtler, W. M. H., *Z. Elektrochem.* **64,** 216 (1960).
12. Sachtler, W. M. H., and Fahrenfort, J., *in* "Actes Deuxieme Congres International de Catalyse," p. 838. Technip, Paris, 1961.
13. Rienäcker, G., and Hansen, N., *Z. Anorg. Chem.* **284,** 162 (1956).
14. Hirota, K., Kuwata, K., and Nakai, Y., *Bull. Chem. Soc. (Japan)* **31,** 861 (1958).
15. Hirota, K., Otaki, T., and Asai, S., *Z. Phys. Chem.* **21,** 438 (1959).
16. Fahrenfort, J., van Reijen, L. L., and Sachtler, W. M. H., *in* "The Mechanism of Heterogeneous Catalysis" (J. H. de Boer, Ed.), p. 23. Elsevier, Amsterdam, 1960.
17. Hirota, K., Kuwata, K., Otaki, T., and Asai, S., *in* "Actes Deuxieme Congres International de Catalyse," p. 809. Technip, Paris, 1961.
18. Eischens, R. E., and Pliskin, W. A., *in* "Actes Deuxieme Congres International de Catalyse," p. 789. Technip, Paris, 1961.
19. Joyner, R. W., and Roberts, M. W., *Proc. Roy. Soc. (London) Sect. A* **350,** 107 (1976).
20. Bond, G. C., "Catalysis by Metals." Academic Press, New York/London, 1962.
21. Mars, P., Scholten, J. J. F., and Zweitering, P., *in* "Advances in Catalysis and Related Subjects," Vol. 14, p. 35. Academic Press, New York/London, 1963.
22. Kaiser, H. J., von Freyberg, H. G., and Doiwa, A., *Z. Naturforsch. B* **26,** 292 (1971).
23. Alsdorf, E., and Volter, J., *Z. Anorg. Chem.* **380,** 303 (1971).
24. Clark, C. H., and Topley, B., *J. Phys. Chem.* **32,** 121 (1928).
25. Rienäcker, G., and Bade, H., *Z. Anorg. Chem.* **248,** 45 (1941).
26. Walton, D. K., and Verhoek, F. H., *in* "Advances in Catalysis and Related Subjects," Vol. 9, p. 682. Academic Press, New York/London, 1957.
27. Inglis, H. S., and Taylor, D., *J. Chem. Soc.*, 2985 (1969).
28. Fukuda, K., Nagishima, S., Noto, Y., Onishi, T., and Tamaru, K., *Trans. Faraday Soc.* **64,** 522 (1968).
29. Szabo, L. G., and Solymosi, F., *in* "Actes Deuxieme Congres International de Catalyse," p. 1627. Technip, Paris, 1961.
30. Platonov, M. S., and Tomilov, V. I., *Zh. Obshchey Khim.* **8,** 346 (1938).
31. Wescott, B. B., and Engelder, C. J., *J. Phys. Chem.* **30,** 476 (1926).
32. Duell, M. J., and Robertson, A. J. B., *Trans. Faraday Soc.* **57,** 1416 (1961).
33. Giner, J., and Rissman, E., *J. Catal.* **9,** 115 (1967).
34. Nagishkina, I. S., and Kiperman, S. L., *Kinet. Katal.* **6,** 1010 (1966).
35. Ruka, R. J., Brockway, L. O., and Boggs, J. E., *J. Amer. Chem. Soc.* **81,** 2930 (1959).
36. Solymosi, F., *in* "Contact Catalysis" (L. G. Szabo, Ed.), p. 395. Elsevier, New York/Amsterdam, 1976.
37. Rienacker, G., and Hansen, N., *Z. Anorg. Chem.* **285,** 283 (1956).

38. Schwab, G. M., and Schwab-Agallidis, E., *Ber. B* **76,** 1228 (1943).
39. Baddour, R. F., and Dalbert, M. C., *J. Phys. Chem.* **70,** 2173 (1966).
40. Criado, J. M., Gonzalez, F., and Trillo, J. M., *J. Catal.* **23,** 11 (1971).
41. Carrion, J., Criado, J. M., Herrera, E. J., and Torres, C., *in* "Proceedings of the Eighth Symposium on the Reactivity of Solids" (N. G. Vannerberg and C. Helgesson, Eds.), p. 267. Plenum, New York, 1976.
42. Kharson, M. S., and Kiperman, S. L., *Dokl. Akad. Nauk. SSSR* **201,** 404 (1971).
43. Dowden, D. A., and Reynolds, P. W., *Disc. Faraday Soc.* **8,** 190 (1950).
44. Quinn, D. F., and Taylor, D., *J. Chem. Soc.*, 5248 (1965).
45. Suhrmann, R., and Wedler, G., *Z. Elektrochem.* **60,** 892 (1956).
46. Rienäcker, G., and Hildebrandt, H., *Z. Anorg. Chem.* **248,** 52 (1941).
47. Fuderer-Leutic, P., and Brihta, I., *Croat. Chim. Acta* **31,** 75 (1959).
48. Kishimoto, S., *J. Phys. Chem.* **77,** 1719 (1973).
49. Schwab, G. M., Block, J., and Schultze, D., *Angew. Chem.* **71,** 101 (1958).
50. Toyama, O., and Kubakawa, Y., *J. Chem. Soc. (Japan)* **74,** 289 (1953).
51. Rienäcker, G., *Z. Elektrochem.* **46,** 369 (1940).
52. Iglesia, E., and Boudart, M., *J. Catal.* **81,** 214 (1983).
53. Iglesia, E., and Boudart, M., *J. Catal.* **81,** 204 (1983).
54. Best, R. J., and Russell, W. W., *J. Amer. Chem. Soc.* **76,** 838 (1954).
55. Rienäcker, G., and Volter, J., *Z. Anorg. Chem.* **302,** 299 (1959).
56. Rienäcker, G., and Volter, J., *Z. Anorg. Chem.* **296,** 210 (1958).
57. Clarke, J. K. A., and Pullin, A. D. E., *Trans. Faraday Soc.* **56,** 534 (1960).
58. Wachs, I. E., and Madix, R. J., *Surf. Sci.* **65,** 287 (1977).
59. Toyoshima, I., and Somorjai, G. A., *Catal. Rev.* **19,** 105 (1979).
60. Iglesia, E., Ph.D. dissertation, Stanford University, 1981.
61. Koros, R. M., and Nowak, E. J., *Chem. Eng. Sci.* **22,** 470 (1967).
62. Madon, R. J., Ph.D. dissertation, Stanford University, 1975.
63. Helms, C. R., and Yu, K. Y., *J. Vac. Sci. Technol.* **12,** 276 (1975).
64. Watanabe, K., Mohri, M., Hashiba, M., and Yamashina, T., *Chem. Lett.* **12,** 1343 (1976).
65. Suhrmann, R., and Wedler, G., *in* "Advances in Catalysis and Related Subjects," Vol. 9, p. 223. Academic Press, New York/London, 1957.
66. Ko, E. I., and Madix, R. J., *Appl. Surf. Sci.* **3,** 236 (1979).
67. Cratty, L. E., and Russell, W. W., *J. Amer. Chem. Soc.* **80,** 767 (1958).
68. Grenoble, D. C., Estadt, M. M., and Ollis, D. F., *J. Catal.* **67,** 90 (1981).
69. Sachtler, W. M. H., *Vide* **164,** 67 (1973).
70. Bircumshaw, L. L., and Edwards, J., *J. Chem. Soc.*, 1800 (1950).
71. Krogmann, K., *Z. Anorg. Chem.* **307,** 16 (1961).
72. Benziger, J. B., Ph.D. dissertation, Stanford University, 1979.
73. Benziger, J. B., Ko, E. I., and Madix, R. J., *J. Catal.* **58,** 149 (1979).
74. Schwab, G. M., and Schmidt, R., *Z. Phys. Chem.* **82,** 174 (1972).